Ferroelectric domain morphologies of (001) $PbZr_{1-x}Ti_xO_3$ epitaxial thin films

Y. L. Li,[a] S. Y. Hu, and L. Q. Chen
Department of Materials Science and Engineering, The Pennsylvania State University, University Park, Pennsylvania 16802

(Received 29 June 2004; accepted 21 November 2004; published online 19 January 2005)

Ferroelectric domain morphologies in (001) $PbZr_{1-x}Ti_xO_3$ epitaxial thin films were studied using the phase-field approach. The film is assumed to have a stress-free top surface and is subject to a biaxial substrate constraint. Both the electrostatic open-circuit and short-circuit boundary conditions on the film surfaces were considered. The phase-field simulations indicated that in addition to the known tetragonal and rhombohedral phases, an orthorhombic phase becomes stable in films under large tensile constraints. The orthorhombic domain structure contains (100) and (010) 90° domain walls and (110) and (1–10) 180° domain walls. For the rhombohedral phase in a thin film, the domain walls are found to be along {101}, (100), and (010) of the prototypical cubic cell. It is shown that the short-circuit boundary condition and compressive substrate constraint enhance the out-of-plane polarization component while the open-circuit boundary condition and tensile substrate constraint suppress it. It is also shown that the depolarization field promotes the formation of herringbonelike morphology for the rhombohedral phase. © *2005 American Institute of Physics*.
[DOI: 10.1063/1.1849820]

I. INTRODUCTION

High remanent polarization, high piezoelectric constant, and relatively low processing temperature make lead zirconate titanate $PbZr_{1-x}Ti_xO_3$ (PZT) films the candidates for nonvolatile ferroelectric random access memory (FeRAM) and ultrahigh-density information storage devices. PZT thin films often have quite different properties from their bulk counterparts due to substrate constraints and finite thickness. Their ferroelectric properties are mainly controlled by the ferroelectric domain structures and their evolution. Therefore, study of ferroelectric domain structure is of both fundamental interest and technological importance and is expected to provide clues to modify ferroelectric properties by heteroepitaxy and strain engineering.

In this work we employ the phase-field approach to investigate the ferroelectric domain morphologies in PZT films. The phase-field approach has been recognized as a powerful tool to predict microstructures during solid phase transformations.[1,2] It does not make any *priori* assumptions on the occurrence of certain phase and domain morphology during the microstructure evolution. The stable microstructure is a direct consequence of minimizing the total free energy. The PZT film considered here is assumed to be a single crystal having a stress-free top surface and subject to a biaxial substrate constraint. Although it is difficult to synthesize single crystals of PZT over a large compositional range across the solid-solution phase diagram, it is possible to grow epitaxial thin films at different compositions.[3–7] The ferroelectric tetragonal domain structures and the resulting properties of $PbTiO_3$ and $PbTiO_3$-rich PZT (e.g., $PbZr_{0.2}Ti_{0.8}O_3$) thin films have been extensively studied by experiments,[8–13] thermodynamic theories,[14–17] and phase-field simulations.[18–21] However, the rhombohedral domain structure in epitaxial thin films is much less well understood although a few attempts have been made to analyze them in both epitaxial thin films[22–24] and bulk ceramics.[25–28] It has been shown previously that in addition to the tetragonal and rhombohedral phases that exist in bulk PZT systems, an orthorhombic phase can be stabilized at certain substrate constraints and temperatures.[29] The main focus of this paper is to study the ferroelectric domain morphologies and domain-wall orientations of the rhombohedral, orthorhombic, and tetragonal domains as a function of composition, temperature, substrate constraint, and electrostatic boundary condition. This paper is organized as follows: in Sec. II, a phase-field model to describe ferroelectric transition and domain structure evolution is described. Section III presents the simulation results on rhombohedral, orthorhombic, and tetragonal domain morphologies. The effect of depolarization field on rhombohedral domain structures is addressed in Sec. IV, and conclusions are summarized in Sec. V.

II. PHASE-FIELD MODEL

In order to describe the ferroelectric transition and domain structures using the phase-field approach, the three components of the space-dependent spontaneous polarization $\mathbf{P}=(P_1,P_2,P_3)$ are chosen as the field variables. The temporal evolution of the polarization field is described by the time-dependent Ginzburg–Landau (TDGL) equations

$$\frac{\partial P_i(\mathbf{x},t)}{\partial t} = -L\frac{\delta F}{\delta P_i(\mathbf{x},t)} \quad (i=1,2,3), \tag{1}$$

where L is a kinetic coefficient which is related to the domain-wall mobility. F is the total free energy of the system. $\delta F/\delta P_i(\mathbf{x},t)$ is the thermodynamic driving force for the spatial and temporal evolution of $P_i(\mathbf{x},t)$. $\mathbf{x}=(x_1,x_2,x_3)$ and t

[a]Electronic mail: yil1@psu.edu

are the spatial coordinate and time, respectively.

The total free energy of a film includes the bulk free energy F_{bulk}, domain-wall energy F_{wall}, elastic energy F_{elas}, and electrostatic energy F_{elec}, i.e.,

$$\begin{aligned} F &= F_{\text{bulk}}(P_i) + F_{\text{wall}}(P_{i,j}) + F_{\text{elas}}(P_i, \varepsilon_{ij}) + F_{\text{elec}}(P_i, E_i) \\ &= \int\int\int_V [f_{\text{bulk}}(P_i) + f_{\text{wall}}(P_{i,j}) + f_{\text{elas}}(P_i, \varepsilon_{ij}) \\ &\quad + f_{\text{elec}}(P_i, E_i)] d^3x, \end{aligned} \tag{2}$$

where V is the volume of the film and $d^3x = dx_1 dx_2 dx_3$. We assume that the strain field ε_{ij} and electric field E_i are always at equilibrium for a given polarization field distribution, i.e., the elastic strain field and electric field of the film are functions of the polarization field.

The bulk free energy density is described by a conventional Landau-type of expansion. For example, a Landau expansion up to sixth order is

$$\begin{aligned} f_{\text{bulk}} &= \alpha_1(P_1^2 + P_2^2 + P_3^2) + \alpha_{11}(P_1^4 + P_2^4 + P_3^4) + \alpha_{12}(P_1^2P_2^2 \\ &\quad + P_2^2P_3^2 + P_3^2P_1^2) + \alpha_{111}(P_1^6 + P_2^6 + P_3^6) + \alpha_{112}[P_1^2(P_2^4 \\ &\quad + P_3^4) + P_2^2(P_1^4 + P_3^4) + P_3^2(P_1^4 + P_2^4)] + \alpha_{123}P_1^2P_2^2P_3^2, \end{aligned} \tag{3}$$

where α_1, α_{11}, α_{12}, α_{111}, α_{112}, and α_{123} are the phenomenological coefficients which determine the nature of the transition, the transition temperature, the spontaneous polarization, and the dielectric susceptibility as a function of temperature in the bulk crystal. It should be emphasized that the set of coefficients are measured under the stress-free boundary condition. The paraelectric state with zero polarization is regarded as a reference for measuring the free energy.

The domain-wall energy can be introduced through the gradients of the polarization field. For a general anisotropic system, the gradient energy density is calculated by

$$f_{\text{wall}} = \tfrac{1}{2} G_{ijkl} P_{i,j} P_{k,l}, \tag{4}$$

where $P_{i,j} = \partial P_i / \partial x_j$ and G_{ijkl} are the gradient energy coefficients. The nonzero components of G_{ijkl} are determined by the symmetry of the parent paraelectric phase. The summation convention for the repeated indices is employed and $i,j,k,l = 1,2,3$. For an isotropic system, it degenerates to

$$\begin{aligned} f_{\text{wall}} &= \tfrac{1}{2} G_{11}(P_{1,1}^2 + P_{1,2}^2 + P_{1,3}^2 + P_{2,1}^2 + P_{2,2}^2 + P_{2,3}^2 + P_{3,1}^2 \\ &\quad + P_{3,2}^2 + P_{3,3}^2), \end{aligned} \tag{5}$$

where G_{ij} are the corresponding gradient coefficient of the Voigt's notation. For instance, $G_{11} = G_{1111}$.

Under the stress-free condition, a ferroelectric phase transition is accompanied by a spontaneous strain, or called eigenstrain in micromechanics,

$$\varepsilon_{ij}^0 = Q_{ijkl} P_k P_l, \tag{6}$$

where Q_{ijkl} is the electrostrictive coefficient tensor. If the interfaces between parent phase and product phase or between different orientation product phases are coherent, elastic strains are generated during the phase transition in order to accommodate the structural changes. The associated elastic energy is calculated by

$$\begin{aligned} f_{\text{elas}} &= \tfrac{1}{2} c_{ijkl} e_{ij} e_{kl} \\ &= \tfrac{1}{2} c_{ijkl}(\varepsilon_{ij} - \varepsilon_{ij}^0)(\varepsilon_{kl} - \varepsilon_{kl}^0) \\ &= \tfrac{1}{2} c_{ijkl}(\varepsilon_{ij} - Q_{ijmn} P_m P_n)(\varepsilon_{kl} - Q_{klmn} P_m P_n) \\ &= \tfrac{1}{2} c_{ijkl} Q_{ijmn} Q_{klst} P_m P_n P_s P_t - c_{ijkl} \varepsilon_{ij} Q_{klmn} P_m P_n \\ &\quad + \tfrac{1}{2} c_{ijkl} \varepsilon_{ij} \varepsilon_{kl}, \end{aligned} \tag{7}$$

where $e_{ij} = \varepsilon_{ij} - \varepsilon_{ij}^0$ is the elastic strain, ε_{ij} is the total strain of the film compared to the parent paraelectric phase, and c_{ijkl} is the elastic stiffness tensor. It is seen that the introduction of elastic energy alters the coefficients of the quadratic and fourth-order terms in the bulk free energy polynomial in Eq. (3). Consequently, the ferroelectric properties of the crystal will be changed if the crystal is clamped. The calculation of the strains and elastic energy in an elastically anisotropic film with a stress-free surface constrained by a much thicker substrate has been discussed in our previous works[18,20] and is based on an analytical solution obtained by combining the mesoscopic elasticity theory of Khachaturyan and Shatalov[30] and Khachaturyan[31] and the Stroh formalism of anisotropic elasticity by Stroh[32] and by Ting.[33]

To consider the dipole-dipole interaction during ferroelectric domain evolution, the electrostatic energy of a domain structure is introduced through

$$f_{\text{elec}} = -\tfrac{1}{2} E_i P_i, \tag{8}$$

where E_i is the dipole electric-field component due to the polarization $\mathbf{P} = (P_1, P_2, P_3)$. The electric field E_i depends on the distribution of the polarization and the boundary conditions on the film surfaces. We assume that the electric field E_i is always at equilibrium for a given polarization field distribution. Calculation of electric fields under the open-circuit surface boundary condition or under given electric potential difference between the top and bottom surfaces is presented in Refs. 19 and 34.

III. FERROELECTRIC DOMAIN MORPHOLOGIES

The temporal evolution of the polarization and thus the domain structures are obtained by numerically solving the TDGL equations in Eq. (1) using the semi-implicit Fourier-spectral method for the time-stepping and spatial discretization.[35] A model size of $128\Delta x \times 128\Delta x \times 36\Delta x$ is employed and periodic boundary conditions are applied along the x_1 and x_2 axes in the film plane. Δx is the space between any two nearest grid points. The thickness of the film is taken as $h_f = 20\Delta x$. In order to include the contribution of substrate deformation to the elastic energy, we allowed the region of the substrate within $h_s = 12\Delta x$ from the substrate-film interface to deform due to the formation of domain structures in the film. Our simulation showed a little change in the results when h_s exceeds about half of the film thickness.[20]

To simulate the domain structures in ferroelectric PZT single-crystal thin films, we employed the bulk free energy and electrostrictive coefficients previously determined by

Haun *et al.*[36–39] (see the Appendix). According to the bulk phase diagram,[40] there is an antiferroelectric transition close to pure $PbZrO_3$ and a transition from the "high-temperature" rhombohedral phase ($F_{R,HT}$, space-group $R3m$) to the "low-temperature" rhombohedral phase ($F_{R,LT}$, space-group $R3c$) through the rotation of oxygen octahedron. The bulk free energy given in Eq. (3) does not incorporate these two transitions. However, we are mostly interested in the ferroelectric domain morphology. The rotation of the oxygen octahedral does not change the nature of the point-group symmetry reduction and so should not affect the specifics of rhombohedral domain formation (space-groups $R3m$ and $R3c$ both have point-group $3m$).[22] Thus, the antiferroelectric transition and the rotation of oxygen octahedron will not be considered in this work.

We assume that the elastic constants are independent of the mole fraction x and have cubic anisotropy. Specifically, we use the values for $PbTiO_3$:[41] $c_{11}=1.75\times10^{11}$ Nm^{-2}, $c_{12}=7.94\times10^{10}$ Nm^{-2}, and $c_{44}=1.11\times10^{11}$ Nm^{-2}. We also assume that the domain-wall energy is isotropic. For convenience, we employ the reduced units in our simulations, $\mathbf{P}^*=\mathbf{P}/P_0$, $\alpha_1^*=\alpha_1/\alpha_0$, $\alpha_{11}^*=\alpha_{11}P_0^2/\alpha_0$, $\alpha_{12}^*=\alpha_{12}P_0^2/\alpha_0$, $\alpha_{111}^*=\alpha_{111}P_0^4/\alpha_0$, $\alpha_{112}^*=\alpha_{112}P_0^4/\alpha_0$, $\alpha_{123}^*=\alpha_{123}P_0^4/\alpha_0$, $G_{11}^*=G_{11}/G_{110}$, $\mathbf{x}^*=\mathbf{x}/l_0$, $\Delta x^*=\Delta x/l_0$, $c_{11}^*=c_{11}/(\alpha_0P_0^2)$, $c_{12}^*=c_{12}/(\alpha_0P_0^2)$, $c_{44}^*=c_{44}/(\alpha_0P_0^2)$, $Q_{11}^*=Q_{11}P_0^2$, $Q_{12}^*=Q_{12}P_0^2$, $Q_{44}^*=Q_{44}P_0^2$, $\omega_0^*=\omega_0\alpha_0$, $\mathbf{E}^*=\mathbf{E}/(\alpha_0P_0)$, $t^*=t\alpha_0L$, where $\alpha_0=|\alpha_1|_{x=1.0,T=25\ ^\circ\mathrm{C}}$, $l_0=\sqrt{G_{110}/\alpha_0}$, $P_0=|P|_{x=1.0,T=25\ ^\circ\mathrm{C}}=0.757$ Cm^{-2} is the spontaneous polarization of bulk $PbTiO_3$ at $T=25\ ^\circ$C, and $\omega_0=8.85\times10^{-12}$ Fm^{-1} is the dielectric permittivity of a vacuum. If $l_0=1$ nm, $G_{110}=1.73\times10^{-10}$ C^{-2} m^4 N. The gradient coefficient $G_{11}^*=0.6$ was used for the simulation. The corresponding wall thickness at $T=25\ ^\circ$C for $PbTiO_3$ is about $1.5\Delta x^*$. The grid space is chosen as $\Delta x^*=1.0$ and the time step is $\Delta t^*=0.1$.

The macroscopic constraint from the substrate is described by the average strain $\overline{\varepsilon}_{\alpha\beta}$ $(\alpha,\beta=1,2)$ while the continuities of the deformation and stresses on the film/substrate interface provide the microscopic constraint. A uniform biaxial constraint of $\overline{\varepsilon}_{11}=\overline{\varepsilon}_{22}=e_0$, and $\overline{\varepsilon}_{12}=0$ is considered. It is known from our previous simulations that the stable ferroelectric phase in the film could be the distorted rhombohedral ($|P_1|=|P_2|>0, |P_3|>0$), orthorhombic ($|P_1|=|P_2|>0, P_3=0$) or tetragonal ($|P_1|>0$, $P_2=P_3=0$ or $|P_2|>0$, $P_1=P_3=0$ or $|P_3|>0$, $P_1=P_2=0$), dependent on the temperature, composition, and substrate constraint e_0.[29] In order to consider the dipole-dipole interactions, the short-circuit surface boundary condition is used in the following domain structure simulations. The short-circuit boundary condition can be achieved by placing top and bottom electrodes when lettinf both electrodes grounded. The electrodes compensate the polarization charges on the surfaces, so no depolarization field develops. In order to calculate the electrostatic field, the relative dielectric constants κ_{ij} of the film are needed.[42] Since κ_{ij} strongly depend on the domain structures in the film, they vary with composition, temperature, as well as the substrate constraint. In the simulations, we approximate κ_{ij} through $\kappa_{ij}=\eta_{ij}/\omega_0$ and $\eta_{ij}=\chi_{ij}^{-1}$ by taking χ_{ij} as the volume average, $\chi_{ij}=1/V\int\int\int_V\partial^2f'/\partial P_i\partial P_jd^3x$,[37] where $f'=f_{\mathrm{bulk}}(P_i)+f_{\mathrm{elas}}(P_i,\varepsilon_{ij})$. It is found that $\kappa_{11}\approx\kappa_{22}$ and $\kappa_{ij}(i\neq j)$ is at least one order of magnitude less than $\kappa_{ii}(i=1,2,3)$. Therefore, we simply take the average of κ_{11} and κ_{22} for κ_{11} and κ_{22}, and $\kappa_{12}=\kappa_{23}=\kappa_{13}=0$ for solving the electrostatic equations.

A. Rhombohedral domain morphology

Based on the bulk PZT phase diagram and the phase diagram of a PZT film under a substrate constraint,[29] the rhombohedral phase is stable at room temperature and a small mole fraction x of $PbTiO_3$. Figure 1 shows three examples of rhombohedral domain morphologies obtained at $x=0.20$ and $T=25\ ^\circ$C. They correspond to three different substrate constraints: (a) $e_0=0.005$, (b) $e_0=0.0$, and (c) $e_0=-0.005$. We started the simulation from a homogeneous paraelectric phase created by assigning each component of the polarization field a zero value at each grid point plus a small random noise of uniform distribution. For all three cases, the initial polarization distribution is the same. The domain structures are plotted using the isosurface of $|P_1^*|=|P_2^*|=P_{10}$, $|P_3^*|=P_{30}$ with the values of P_{10}, P_{30} listed below the figures.

According to the symmetry relationship between the cubic paraelectric crystal and the rhombohedral ferroelectric state, there are eight crystallographically distinct variants of noncentrosymmetric rhomboheral domains with the polarizations along the $\langle111\rangle$ directions of the parent cubic phase. However, only four of the eight variants have a unique deformation state with respect to the prototype since the spontaneous strains for positive and negative polarizations are the same. It has been shown previously that the possible orientations of twin domain walls that separate the four rhombohedral variants are {100} and {110}.[22,25–28] In order to maintain the charge neutrality for the domain wall, the normal component of the polarization vector needs to be conserved across the domain wall. Since the short-circuit electrostatic boundary was employed in the simulation, there will be no polarization charges in the out-of-plane direction. Therefore, the short-circuit electrostatic boundary condition promotes the film being poled in the out-of-plane direction, which can be seen from Fig. 1 where $P_3>0$ through the whole film. The corresponding domain walls shown in Fig. 1 are, respectively, parallel to planes (-101) and $(0-11)$, which is consistent with the theoretical analysis.

It should be emphasized that because of the biaxial substrate constraint, the magnitude of the out-of-plane component, P_3, is different from the in-plane components, P_1 and P_2, i.e., $|P_1|=|P_2|\neq|P_3|$. As a result, the {011} domain walls deviate slightly from the ideal 45° direction. As shown in Fig. 1, a compressive constraint decreases the angle between the domain wall and film/substrate interface whereas a tensile constraint enlarges it.

We calculated the volume average of the polarization component over the domain structure and obtained the following values for the three different substrate constraints: (a) $\overline{|P_1^*|}=0.377$, $\overline{|P_2^*|}=0.392$, $\overline{|P_3^*|}=0.334$; (b) $\overline{|P_1^*|}=0.341$, $\overline{|P_2^*|}=0.333$, $\overline{|P_3^*|}=0.379$; and (c) $\overline{|P_1^*|}=0.262$, $\overline{|P_2^*|}=0.252$, $\overline{|P_3^*|}=0.431$. It is seen that $\overline{|P_1^*|}$ and $\overline{|P_2^*|}$ are close to each other but different from $\overline{|P_3^*|}$ because of the uniform biaxial con-

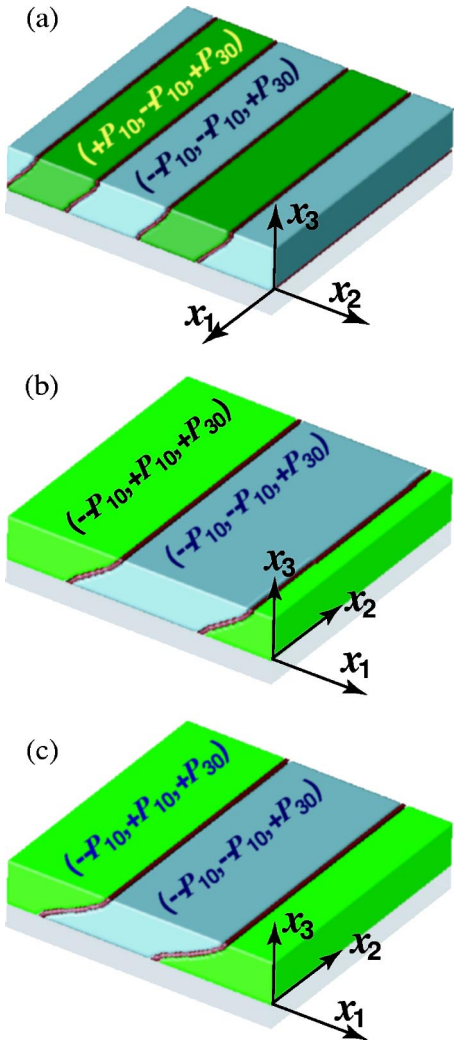

FIG. 1. Rhombohedral domain morphologies in $PbZr_{0.8}Ti_{0.2}O_3$ films at $T=25\ ^\circ C$. (a) $e_0=0.005$, $\kappa_{11}=\kappa_{22}=177.3$, $\kappa_{33}=221.9$; $P_{10}=0.32$, $P_{30}=0.29$; (b) $e_0=0.00$, $\kappa_{11}=\kappa_{22}=233.4$, $\kappa_{33}=188.2$; $P_{10}=0.31$, $P_{30}=0.36$; and (c) $e_0=-0.005$, $\kappa_{11}=\kappa_{22}=396.9$, $\kappa_{33}=165.7$; $P_{10}=0.20$, $P_{30}=0.42$.

straint. Obviously, the compressive substrate constraint increases $|\overline{P_3^*}|$ while tensile constraint suppresses it. The distortion of the rhombohedral phase by the substrate constraint also leads to anisotropic dielectric constants, i.e., $\kappa_{11}=\kappa_{22}\neq\kappa_{33}$, which can be easily seen from the values listed in the figure caption. Therefore, it is possible to use the substrate constraint to modify the dielectric constants and polarization magnitude.

B. Orthorhombic domain morphology

Under a large tensile substrate constraint, the orthorhombic phase with polarization of $|P_1|=|P_2|>0$ and $P_3=0$ can be stabilized at higher temperature in a PZT film with small mole fraction of $PbTiO_3$.[29] There are four variants for the orthorhombic phase, i.e., $(P_1,P_1,0)$, $(P_1,-P_1,0)$, $(-P_1,P_1,0)$, and $(-P_1,-P_1,0)$. These variants form 90° domain walls of {100} orientation or 180° domain walls along {110}.[25] Figure 2 shows two examples of orthorhombic domain structures obtained at $x=0.20$, $T=280\ ^\circ C$, and $e_0=0.005$. The two domain structures correspond to two different initial random polarization distributions. The polarization

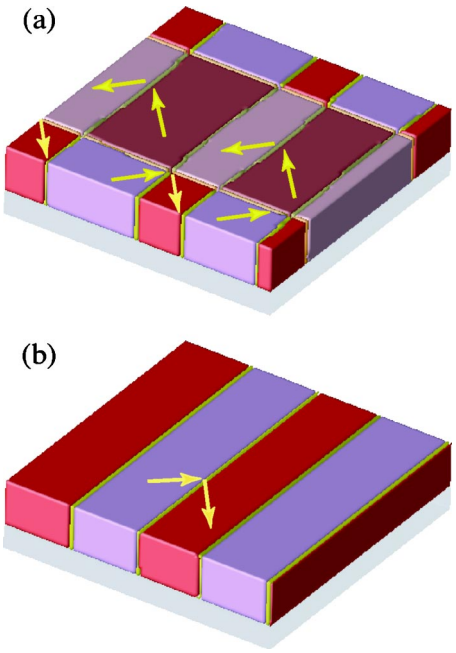

FIG. 2. Orthorhombic domain morphologies in $PbZr_{0.8}Ti_{0.2}O_3$ films at $T=280\ ^\circ C$ and $e_0=0.005$. (a) $\kappa_{11}=\kappa_{22}=700.6$, $\kappa_{33}=2404$ and (b) $\kappa_{11}=\kappa_{22}=668.0$, $\kappa_{33}=2417$.

directions in each domain are shown. It is observed that the polarization configures across the domains are all of head-to-tail arrangements, consistent with electrostatic energy minimization. Although Figs. 2(a) and 2(b) look quite different, they have similar domain shapes and almost the same dielectric constants. The relatively high dielectric constants are due to the fact that the temperature is near the ferroelectric transition temperature. It should be pointed out that although the orthorhombic phase has been predicted from the simulation based on the thermodynamic parameters given by Haun *et al.*,[36–39] it has not yet been confirmed by experiments.

C. Tetragonal domain morphology

Tetragonal domain structures are probably the most often studied in experiments. Based on the phase stability map,[29] the tetragonal phase is stable in a PZT film with mole fraction of $PbTiO_3$ $x>0.5$. It has been shown that the stable region of the tetragonal phase extends to the range of $x<0.5$ under a substrate constraint regardless whether it is tensile or compressive. There are totally six variants of tetragonal phase. They are $(\pm P_1,0,0)$, $(0,\pm P_2,0)$, and $(0,0,\pm P_3)$, respectively. Due to the biaxial substrate constraint and the electrostatic boundary condition, P_3 is different from P_1 and P_2 but $|P_1|=|P_2|$, similar to the case of rhombohedral domains. Conventionally, the domains with polarization $(\pm P_1,0,0)$, $(0,\pm P_2,0)$, and $(0,0,\pm P_3)$ are called a_1 domain, a_2 domain, and c domain, respectively. The interfaces between these variants are the 90° domain walls along {110}.

Figure 3 shows two tetragonal domain structures for two different substrate constraints, $e_0=0.001$ and $e_0=0.01$, in a $PbZr_{0.2}Ti_{0.8}P_3$ film at $T=25\ ^\circ C$. The three colors represent the a_1, a_2, and c domains, respectively. The domain-wall orientations are well defined in the simulated domain struc-

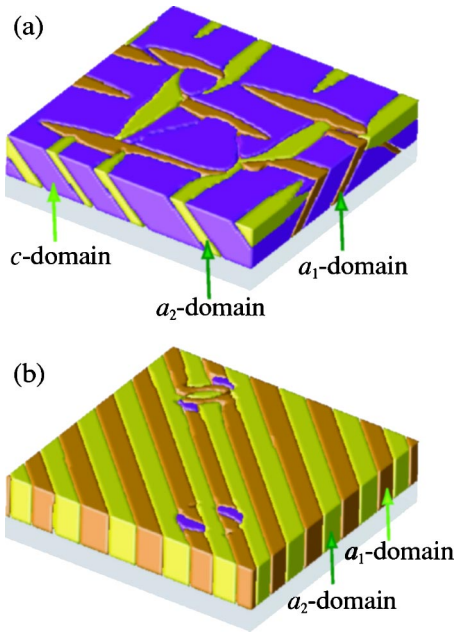

FIG. 3. Tetragonal domain morphologies in $PbZr_{0.2}Ti_{0.8}O_3$ films at $T=25\ ^\circ C$ with (a) $e_0=0.001$ and (b) $e_0=0.01$.

tures. As expected, under a biaxial substrate constraint, the volume fractions of a_1 and a_2 domains are approximately the same, and they increase with the tensile strain e_0. For example, for the two domain structures in Fig. 3, the corresponding domain volume fractions are, respectively, $Va_1=0.177$, $Va_2=0.179$, and $Vc=0.644$ for $e_0=0.001$ and $Va_1=0.493$, $Va_2=0.505$, and $Vc=0.002$ for $e_0=0.01$. The dielectric constants corresponding to the domain structures are $\kappa_{11}=\kappa_{22}=135.6$, $\kappa_{33}=71.4$ for $e_0=0.001$ and $\kappa_{11}=\kappa_{22}=80.5$, $\kappa_{33}=169.6$ for $e_0=0.01$. Therefore, one can see that the out-of-plane dielectric constant κ_{33} has a larger value in a film dominated by a_1/a_2 domains than that in the film where c domain is the majority.

IV. EFFECT OF DEPOLARIZATION FIELD ON RHOMBOHEDRAL DOMAINS

The results presented in Sec. III were obtained under the short-circuit electrostatic boundary condition, and hence no depolarization field between the top and bottom film surfaces exists. To study the effect of electric boundary conditions on the domain structure, we also consider the open-circuit boundary condition for the film surfaces. The domain structure of a $PbZr_{0.8}Ti_{0.2}O_3$ film at temperature $T=25\ ^\circ C$ and substrate constraint $e_0=0.005$ is shown in Fig. 4.

The domain structure in Fig. 4(a) was obtained by directly applying the open-circuit electrostatic surface boundary condition. The dielectric constants $\kappa_{11}=\kappa_{22}$ and κ_{33} are evaluated using the same method discussed in Sec. III, and $\kappa_{11}=\kappa_{22}=202.4$, $\kappa_{33}=493.2$ for the final domain structure at the end of the simulation. It shows a herringbonelike morphology and is very different from the one shown in Fig. 1(a) although the only difference between the two simulations is the different electrostatic boundary conditions. From Fig. 4(a) one can see that all the domain walls are perpendicular to the film/substrate interface. The results showed that the

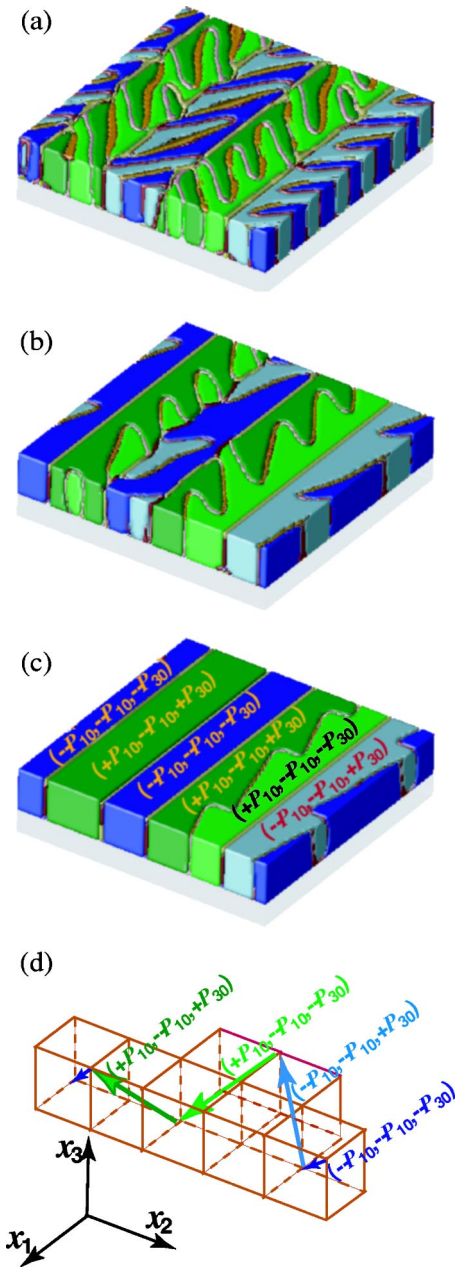

FIG. 4. (a–c) Rhombohedral domain morphologies in $PbZr_{0.8}Ti_{0.2}O_3$ films at $T=25\ ^\circ C$ and $e_0=0.005$ under the open-circuit surface boundary condition and (d) schematic illustrations of the polarization directions and components.

volume average of the polarization component P_3 was close to zero, which corresponds to an unpoled state in the out-of plane direction.[22] In order to understand the driving forces that are responsible for the formation of herringbonelike morphology, we artificially increased the value of κ_{33}. Figures 4(b) and 4(c) display the domain structures obtained by fixing $\kappa_{11}=\kappa_{22}=200$ and taking $\kappa_{33}=1000$ and 1500, respectively. As one can see that the larger the κ_{33}, the weaker the effect of the open-circuit boundary condition is. The herringbonelike morphology gradually disappears with the increase of κ_{33}. From these simulations, we may conclude that the herringbonelike morphology is due to the effect of strong depolarization field. Herringbonelike morphology was often experimentally observed in bulk systems[27,28] but has not

been reported for films. As shown in the schematic polarization arrangement in Fig. 4(d), the herringbonelike morphology consists of (110) and (1–10) domain walls which were previously predicted to be unfavorable wall orientations in (001) PZT films.[22]

The impact of the open-circuit boundary condition on tetragonal domain structures was shown to be similar to that in lead titanate films.[19] For the orthorhombic domain structures, the film surface boundary condition does not have a significant effect since the polarization in the orthorhombic phase is in plane and perpendicular to the depolarization field from the open-circuit boundary condition.

V. SUMMARIES AND CONCLUSIONS

A phase-field model is employed to simulate the ferroelectric domain morphologies in (001) $PbZr_{1-x}Ti_xO_3$ (PZT) epitaxial thin films. The electrostatic short-circuit and open-circuit surface boundary conditions are considered. The {100} and {110} domain walls between different rhombohedral variants, the 90° domain walls oriented along {100} between the orthorhombic variants having in-plane polarization, and the 90° domain walls between the tetragonal variants were predicted from the simulations. It is found that both the substrate constraint and the electrostatic boundary condition can significantly alter the orientation and magnitude of the polarization, domain morphologies, as well as the ferroelectric properties. The simulation results may provide insight for strain engineering of PZT ferroelectric films.

ACKNOWLEDGMENT

The financial supports from the National Science Foundation under Grant Nos. DMR-0122638 and DMR-0103354 are gratefully acknowledged.

APPENDIX

The relative coefficients are calculated by

$$Q_{11} = \frac{0.029578}{1 + 200(x - 0.5)^2} + 0.042796x + 0.045624,$$

$$Q_{12} = \frac{0.026568}{1 + 200(x - 0.5)^2} - 0.012093x - 0.013386,$$

$$Q_{44} = \frac{1}{2}\left[\frac{0.025325}{1 + 200(x - 0.5)^2} + 0.020857x + 0.046147\right],$$

$$\alpha_1 = (T - T_0)/(2\omega_0 C_0),$$

$$\alpha_{11} = (10.612 - 22.655x + 10.955x^2) \times 10^{13}/C_0,$$

$$\alpha_{111} = (12.026 - 17.296x + 9.179x^2) \times 10^{13}/C_0,$$

$$\alpha_{112} = (4.2904 - 3.3754x + 58.804e^{-29.397x}) \times 10^{14}/C_0,$$

$$\alpha_{12} = \eta_1/3 - \alpha_{11}, \quad \alpha_{123} = \eta_2 - 3\alpha_{111} - 6\alpha_{112},$$

$$\eta_1 = [2.6213 + 0.42743x - (9.6 + 0.012501x)e^{-12.6x}] \times 10^{14}/C_0,$$

$$\eta_2 = [0.887 - 0.76973x + (16.225 - 0.088651x)e^{-21.255x}] \times 10^{15}/C_0,$$

$$T_0 = 189.48 + 843.4x - 2105.5x^2 + 4041.8x^3 - 3828.3x^4 + 1337.8x^5,$$

$$C_0 = \left[\frac{2.1716}{1 + 500.05(x - 0.5)^2} + 0.131x + 2.01\right] \times 10^5 \quad \text{when } 0.0 \leqslant x \leqslant 0.5,$$

$$C_0 = \left[\frac{2.8339}{1 + 126.56(x - 0.5)^2} + 1.4132\right] \times 10^5, \quad \text{when } 0.5 \leqslant x \leqslant 1.0,$$

where x is the mole fraction of $PbTiO_3$ in PZT and ω_0 is the dielectric permittivity of a vacuum. The units are in SI units and temperature is in °C. Some typos of the coefficients in the original published articles were corrected here.

[1] L. Q. Chen and Y. Z. Wang, JOM **48**, 13 (1996).
[2] L. Q. Chen, Annu. Rev. Mater. Res. **32**, 113 (2002).
[3] R. Takayama and Y. Tomita, J. Appl. Phys. **65**, 1666 (1989).
[4] C. M. Foster, G. R. Bai, R. Csencsits, J. Vetrone, R. Jammy, L. A. Wills, E. Carr, and J. Amano, J. Appl. Phys. **81**, 2349 (1997).
[5] J. G. Hong, H. W. Song, S. B. Hong, H. Shin, and K. No, J. Appl. Phys. **92**, 7434 (2002).
[6] T. Oikawa, M. Aratani, H. Funakubo, K. Saito, and M. Mizuhira, J. Appl. Phys. **95**, 3111 (2004).
[7] I. Kanno, H. Kotera, K. Wasa, T. Matsunaga, T. Kamada, and R. Takayama, J. Appl. Phys. **93**, 4091 (2003).
[8] A. Seifert, F. F. Lange, and J. S. Speck, J. Mater. Res. **10**, 680 (1995).
[9] J. S. Speck, A. Seifert, W. Pompe, and R. Ramesh, J. Appl. Phys. **76**, 477 (1994).
[10] C. M. Foster *et al.*, J. Appl. Phys. **78**, 2607 (1995).
[11] S. P. Alpay, V. Nagarajan, L. A. Bendersky, M. D. Vaudin, S. Aggarwal, R. Ramesh, and A. L. Roytburd, J. Appl. Phys. **85**, 3271 (1999).
[12] A. L. Roytburd, S. P. Alpay, L. A. Bendersky, V. Nagarajan, and R. Ramesh, J. Appl. Phys. **89**, 553 (2001).
[13] C. S. Ganpule *et al.*, J. Appl. Phys. **91**, 1477 (2002).
[14] J. S. Speck and W. Pompe, J. Appl. Phys. **76**, 466 (1994).
[15] A. L. Roytburd, J. Appl. Phys. **83**, 228 (1998).
[16] A. L. Roytburd, J. Appl. Phys. **83**, 239 (1998).
[17] S. P. Alpay and A. L. Roytburd, J. Appl. Phys. **83**, 4714 (1998).
[18] Y. L. Li, S. Y. Hu, Z. K. Liu, and L. Q. Chen, Appl. Phys. Lett. **78**, 3878 (2001).
[19] Y. L. Li, S. Y. Hu, Z. K. Liu, and L. Q. Chen, Appl. Phys. Lett. **81**, 427 (2002).
[20] Y. L. Li, S. Y. Hu, Z. K. Liu, and L. Q. Chen, Acta Mater. **50**, 395 (2002).
[21] S. Y. Hu, Y. L. Li, and L. Q. Chen, J. Appl. Phys. **94**, 2542 (2003).
[22] S. K. Streiffer *et al.*, J. Appl. Phys. **83**, 2742 (1998).
[23] A. E. Romanov, M. J. Lefevre, J. S. Speck, W. Pompe, S. K. Streiffer, and C. M. Foster, J. Appl. Phys. **83**, 2754 (1998).
[24] Q. Tan, Z. Xu, and D. Viehland, J. Mater. Res. **14**, 4251 (1999).
[25] F. Jona and G. Shirane, *Ferroelectric Crystals* (Pergamon, Oxford, 1962).
[26] J. Fousek and V. Janovec, J. Appl. Phys. **40**, 135 (1969).
[27] C. A. Randall, D. J. Barber, and R. W. Whatmore, J. Mater. Sci. **22**, 925 (1987).
[28] J. Ricote, R. W. Whatmore, and D. J. Barber, J. Phys.: Condens. Matter **12**, 323 (2000).
[29] Y. L. Li, S. Choudhury, Z. K. Liu, and L. Q. Chen, Appl. Phys. Lett. **83**, 1608 (2003).
[30] A. G. Khachaturyan and G. A. Shatalov, Sov. Phys. JETP **29**, 557 (1969).
[31] A. G. Khachaturyan, *Theory of Structural Transformation in Solids*

(Wiley, New York, 1983).
[32]A. N. Stroh, J. Math. Phys. **41**, 77 (1962).
[33]T. C. T. Ting, *Anisotropic Elasticity: Theory and Applications* (Oxford University Press, 1996).
[34]Y. L. Li, L. Q. Chen, G. Asayama, D. G. Schlom, M. A. Zurbuchen, and S. K. Streiffer, J. Appl. Phys. **95**, 6332 (2004).
[35]L. Q. Chen and J. Shen, Comput. Phys. Commun. **108**, 147 (1998).
[36]M. J. Haun, Ph.D. thesis, The Pennsylvania State University, 1988.
[37]M. J. Haun, E. Furman, S. J. Jang, and L. E. Cross, Ferroelectrics **99**, 13 (1989).
[38]M. J. Haun, E. Furman, H. A. McKinstry, and L. E. Cross, Ferroelectrics **99**, 27 (1989).
[39]M. J. Haun, Z. Q. Zhuang, E. Furman, S. J. Jang, and L. E. Cross, Ferroelectrics **99**, 45 (1989).
[40]B. Jaffe, W. J. Cook, and H. Jaffe, *Piezoelectric Ceramics* (Academic, London, 1971).
[41]N. A. Pertsev, A. G. Zembilgotov, and A. K. Tagantsev, Phys. Rev. Lett. **80**, 1988 (1998).
[42]D. R. Tilley, in *Ferroelectric Ceramics: Tutorial Reviews, Theory, Processing, and Applications*, edited by N. Setter and E. L. Colla (Birkhaueser, Boston, 1993), pp. 163–183.